

# Molecular Beam Epitaxy Grown $\text{Cr}_2\text{Te}_3$ Thin Films with Tunable Curie Temperatures for Spintronic Devices

Hongxi Li,<sup>†,‡,§,||D</sup> Linjing Wang,<sup>†,§</sup> Junshu Chen,<sup>†,¶,||D</sup> Tao Yu,<sup>†</sup> Liang Zhou,<sup>†</sup> Yang Qiu,<sup>†</sup> Hongtao He,<sup>†</sup> Fei Ye,<sup>†</sup> Iam Keong Sou,<sup>\*,‡</sup> and Gan Wang<sup>\*,†,§,||D</sup>

<sup>†</sup>Institute for Quantum Science and Engineering, and Department of Physics, Southern University of Science and Technology, 1088 Xueyuan Avenue, Shenzhen 518055, China

<sup>‡</sup>Department of Physics, The Hong Kong University of Science and Technology, Hong Kong 999077, China

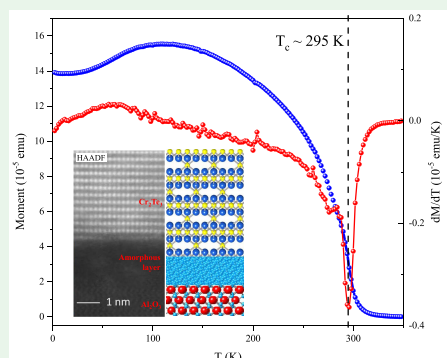
<sup>¶</sup>Department of Physics, National University of Singapore, 2 Science Drive 3, Singapore 117551, Singapore

<sup>\*</sup>Shenzhen Key Laboratory of Quantum Science and Engineering, 1088 Xueyuan Avenue, Shenzhen 518055, China

## S Supporting Information

**ABSTRACT:** Materials that have a perpendicular magnetic anisotropy (PMA) effect with a high Curie temperature are essential in spintronics applications.  $\text{Cr}_2\text{Te}_3$  is a transition-metal chalcogenide that demonstrates a PMA effect but with a relatively low Curie temperature of about 180 K, significantly limiting its practical application. In this work, we reported the epitaxial growth of  $\text{Cr}_2\text{Te}_3$  thin films on  $\text{Al}_2\text{O}_3$  substrates with a Curie temperature ranging from 165 to 295 K, closely dependent on the thicknesses and lattice constants of the thin films. To study the physical origin of the improved Curie temperature, structural analysis, magneto-transport, and magnetic characterizations were conducted and analyzed in detail. In contrast with previous reports, all the high Curie temperature thin films have electron type carriers instead of hole carriers, which is possibly caused by the Al diffusion from the  $\text{Al}_2\text{O}_3$  substrate. On the basis of the structure and chemical analysis, a phenomenological model based on the degree of coupling between ferromagnetic and antiferromagnetic ordering, hosted by the fully occupied and with-vacancy Cr layer alternatively, was proposed to explain the observed Curie temperature enhancement in our samples. These findings indicate that the Curie temperature of  $\text{Cr}_2\text{Te}_3$  thin films may potentially be tuned by Al doping, performing as a novel magnetic material suitable for various magnetic applications.

**KEYWORDS:** NiAs-type  $\text{Cr}_2\text{Te}_3$ , molecular beam epitaxy, high Curie temperature, perpendicular magnetic anisotropy, Al doping, anomalous Hall effect



## INTRODUCTION

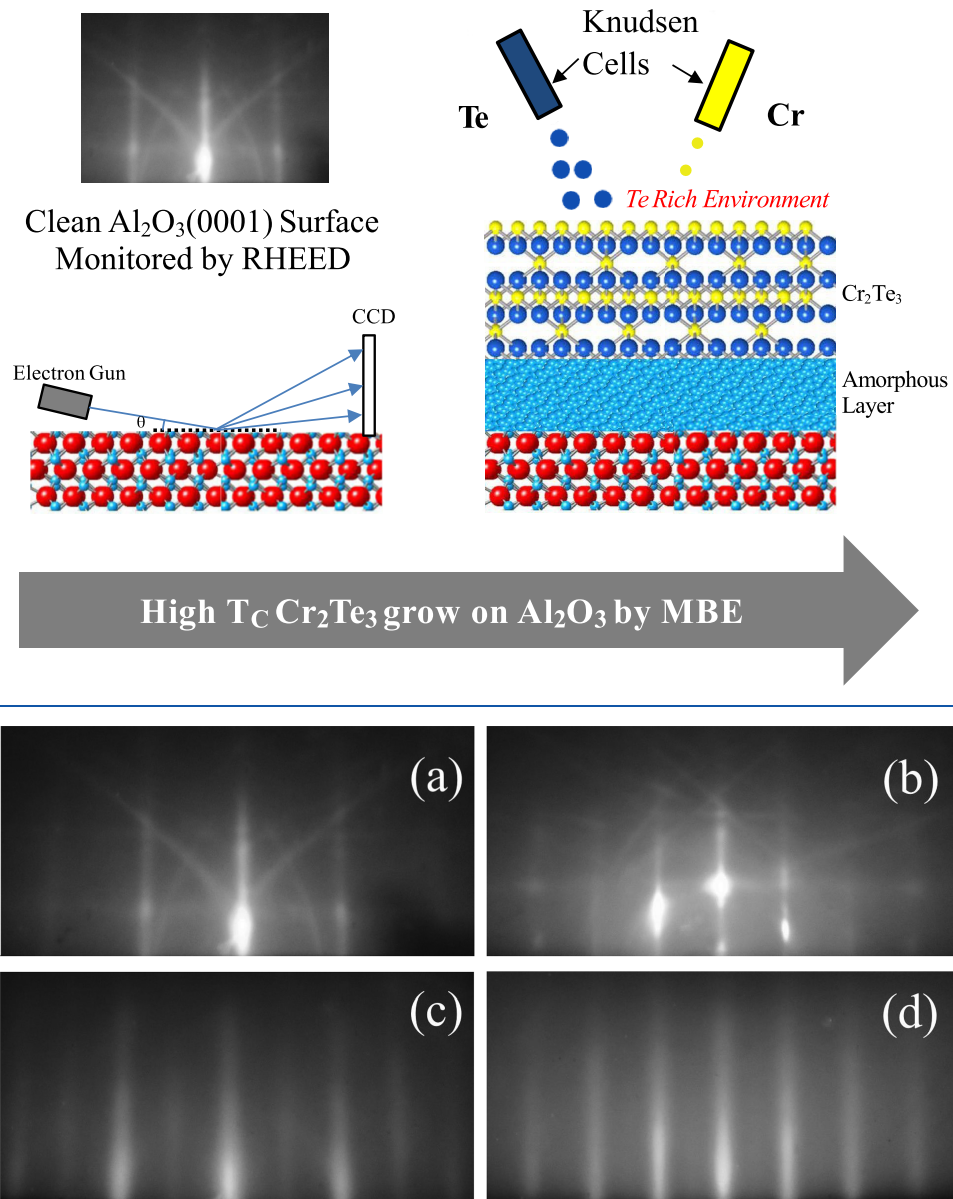
Being a typical transition metal chalcogenide, chromium telluride possesses a large family of compounds in the bulk state. All these compounds have hexagonal structure and ferromagnetic ordering at stable states with a wide range of Curie temperature from 170 to 340 K, depending sensitively on the atomic ratio between Cr and Te. In the bulk state, the chromium telluride with a Cr/Te ratio around 1:1 has the highest Curie temperature around 340 K,<sup>1–3</sup> while the other phases of chromium telluride with Cr vacancy around 0.1 to 0.33 have a Curie temperature between 150 and 340 K. Not only the Curie temperature but also the magnetic anisotropy of the chromium telluride compounds depends on the stoichiometric ratio as well as the lattice structure intimately, in which only the phase with  $\text{Cr}_2\text{Te}_3$  has stable perpendicular magnetic anisotropy in thin film form.<sup>4,5</sup> In the past decade, many efforts had been made on the growth of chromium telluride thin films on semiconducting substrates. For example, structural and magnetic properties of hexagonal  $\text{Cr}_2\text{Te}_3$  films grown on  $\text{CdTe}(001)$  with Curie temperature of 175 K has been studied

by Ken Kanazawa et al.<sup>6</sup> A perpendicular magnetic anisotropy (PMA) and spin-glass-like behavior of hexagonal  $\text{Cr}_2\text{Te}_3$  grown on  $\text{Al}_2\text{O}_3(0001)$  and  $\text{Si}(111)$  substrates with Curie temperature of about 180 K were studied systematically.<sup>7,8</sup> The thin  $\text{Cr}_2\text{Te}_3$  ferromagnetic metallic film was used in a field effect capacitor (FEC) structure at a temperature of 175 K.<sup>9</sup> Saito et al. have studied tunneling magnetoresistance (TMR) in the magnetic tunneling junctions (MTJs) with  $\text{Cr}_{1-\delta}\text{Te}$  being one of the electrodes around 170 K.<sup>10</sup> Especially, in the recent research, the  $\text{Cr}_2\text{Te}_3$ 's strong PMA has been widely integrated in the interface engineering for realizing non trivial topological spin textures, such as the magnetic skyrmions,<sup>11–13</sup> encouragingly showing that the hexagonal phase  $\text{Cr}_{1-\delta}\text{Te}$  thin films possess promising potentials for the application in the spintronic and spin transfer torque (STT) devices development. However, the Curie temperature of the epitaxially grown

Received: June 21, 2019

Accepted: October 25, 2019

Published: October 25, 2019

Scheme 1. Schematics of High Curie Temperature  $\text{Cr}_2\text{Te}_3$  Thin Films Grown on  $\text{Al}_2\text{O}_3$  by Molecular Beam Epitaxy (MBE)

**Figure 1.** RHEED patterns observed for the growth of a typical  $\text{Cr}_2\text{Te}_3$  thin film. (a,b) RHEED patterns from a clean  $\text{Al}_2\text{O}_3$  (0001) surface with the incident electron beam along the  $[10\bar{1}0]$  and  $[11\bar{2}0]$  orientations of  $\text{Al}_2\text{O}_3$ , respectively; (c,d) Corresponding RHEED patterns from the  $\text{Cr}_2\text{Te}_3$  surface along the same orientations.

chromium telluride thin films with strong PMA is still desired to be further improved for fabricating reliable devices working at room temperature.

Even though the Curie temperature ( $T_C$ ) for bulk hexagonal phase  $\text{Cr}_{1-\delta}\text{Te}$  can reach as high as 340 K when the Cr/Te ratio reaches 1:1, their easy axis is orthogonal to the  $c$ -axis, which made it unlikely to be grown with strong PMA in devices.<sup>1,14</sup> Several works have been reported for the growth of Zinc blende  $\text{CrTe}$  on GaAs (001) substrate with ZnTe or CdTe buffer layer.<sup>9,15–17</sup> However, the fragile nature of the zinc blend structure strongly prevents its practical application. Hereby, we report that  $\text{Cr}_2\text{Te}_3$  thin films with a stable NiAs-type hexagonal structure are grown on  $\text{Al}_2\text{O}_3$  (0001) substrates

by the molecular beam epitaxy (MBE) technique with high Curie temperature. Thorough studies on the strain and lattice constants show that the Curie temperature is sensitively determined by the spacing of (001) plane of  $\text{Cr}_2\text{Te}_3$  thin films. To the best of our knowledge, our work achieved the highest Curie temperature for NiAs-type chromium telluride thin films grown by epitaxial schemes, which paves the way for the fabrication of chalcogenide-based spintronic devices working at near ambient conditions.

## EXPERIMENTAL DETAILS

[001] oriented  $\text{Cr}_2\text{Te}_3$  thin films were grown on epi-ready  $\text{Al}_2\text{O}_3$ (0001) substrates (HF-Kejing, China) in a customized MBE

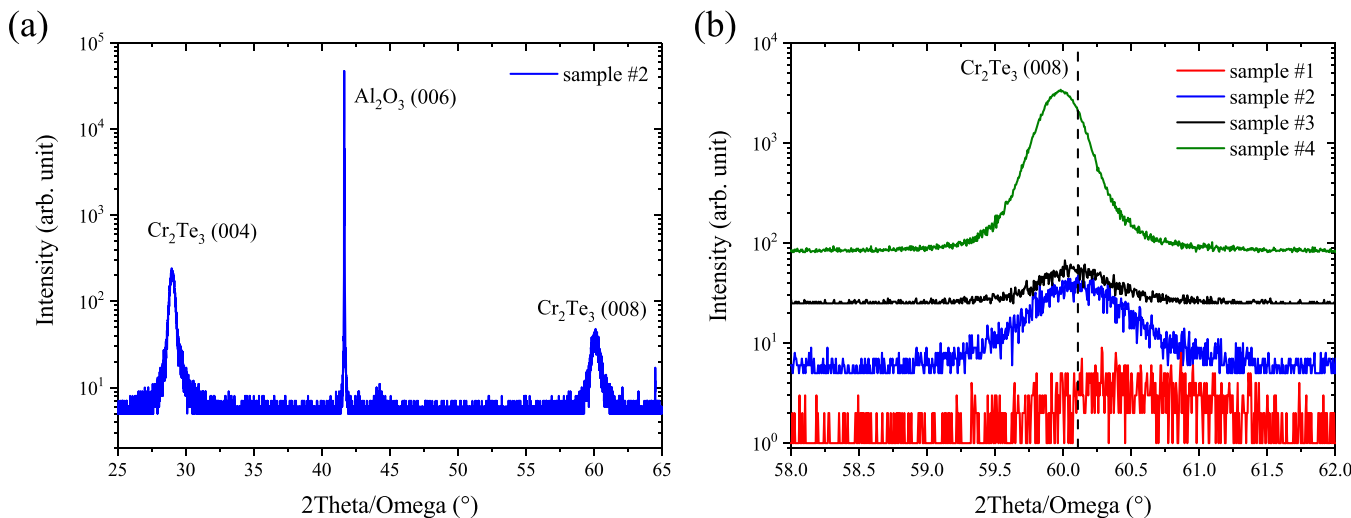


**Figure 2.** X-ray diffraction (XRD) profiles of Cr<sub>2</sub>Te<sub>3</sub> thin films. (a) XRD profile of sample #2; (b) XRD profiles of the (008) peak of Cr<sub>2</sub>Te<sub>3</sub> thin films with increasing thickness.

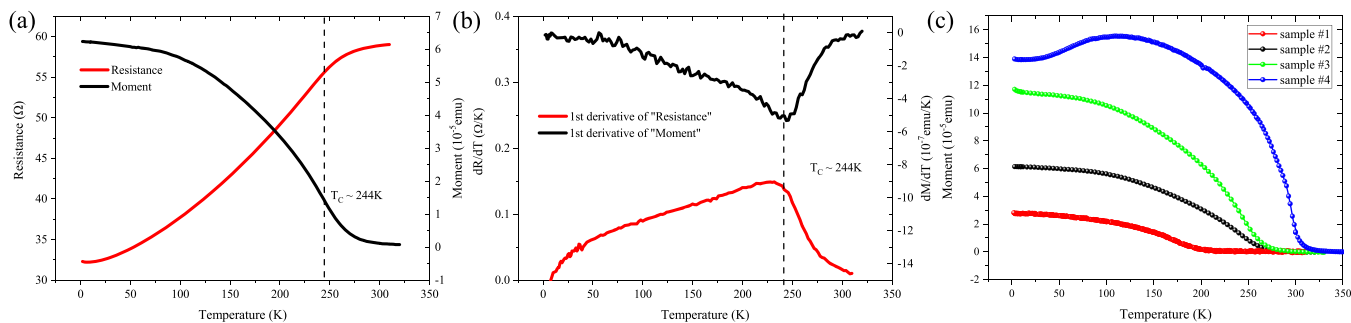


**Figure 3.** Magnetization characterization of sample #1–#4. (a) R–T and M–T curves of sample #2; (b) First derivation of R–T and M–T curves of sample #2; (c) M–T curves measured for samples #1–#4 with magnetic field perpendicular to the surface, in which the applied field for sample #1–#3 is 1000 Oe, except 50 Oe for sample #4.

system with base ultrahigh vacuum better than  $1 \times 10^{-10}$  Torr, equipped with a 15 keV reflective high energy electron diffraction (RHEED) for monitoring the epitaxy. Before growth, Al<sub>2</sub>O<sub>3</sub>(0001) substrates were annealed at 600 °C for 15 min for degassing. Chromium (99.999% Goodfellow UK) and tellurium (99.999% Goodfellow UK) were evaporated by two Knudsen-type effusion cells for providing independent fluxes, respectively, and codeposited on the substrate at 370 °C, as shown in Scheme 1. The flux ratio between chromium and tellurium atom was determined to be around 1:7. Ex situ thickness characterization is done by atomic force microscopy (AFM) and X-ray reflectometry (XRR), indicating that the growth rate was about 1 nm/min. To investigate the property of Cr<sub>2</sub>Te<sub>3</sub> grown on Al<sub>2</sub>O<sub>3</sub> substrates systematically, several Cr<sub>2</sub>Te<sub>3</sub> samples with different thicknesses named as sample #1 (15 nm), #2 (30 nm), #3 (45 nm), and #4 (300 nm) are reported in this work.

A Rigaku high-resolution X-ray diffractometer (XRD), Talos transmission electron microscope (TEM) coupled with energy dispersive X-ray spectrometer (EDX), and FEI Titan Spherical aberration corrected scanning transmission electron microscope (STEM) were employed to study the lattice structures and chemical compositions of the as-grown chromium telluride thin films (the detail stoichiometry analysis of Cr<sub>2</sub>Te<sub>3</sub> can be found in section S1 in the Supporting Information). The magnetic properties were studied using Quantum Design superconducting quantum interference device (SQUID). Transport properties are measured using an Oxford Physical Property Measurement System (PPMS).

## RESULTS AND DISCUSSION

Figure 1 displays the RHEED patterns observed for the growth of a typical Cr<sub>2</sub>Te<sub>3</sub> thin film sample. Panels a and b of Figure 1 are the RHEED patterns of a cleaned Al<sub>2</sub>O<sub>3</sub>(0001) surface along the [10̄10] and [11̄20] electron beam incidence, respectively, after a preheat treatment. Kikuchi lines can be clearly seen in these patterns, indicating a clean and smooth surface morphology of the substrate was achieved. Corresponding RHEED patterns observed after the growth of a Cr<sub>2</sub>Te<sub>3</sub> thin film are shown in Figure 1c,d. Half-order reconstruction lines are seen in both patterns, reflecting that the as-grown Cr<sub>2</sub>Te<sub>3</sub> thin film has a high crystalline quality. The long streaky patterns were being maintained during the entire Cr<sub>2</sub>Te<sub>3</sub> growth process, suggesting that its growth was via a two-dimensional growth mode with an atomically flat surface.

Figure 2a shows the XRD profile of sample #2, showing a typical result for the Cr<sub>2</sub>Te<sub>3</sub> thin film samples presented in this work. The layer peaks (004) and (008) in Figure 2a match well with the hexagonal structure of Cr<sub>2</sub>Te<sub>3</sub> oriented along the [001] direction, while the (006) peak is from the Al<sub>2</sub>O<sub>3</sub> substrate. The derived c-lattice parameter is 12.985 Å for Al<sub>2</sub>O<sub>3</sub>, same as the standardized database in Springer Materials.<sup>18</sup> The c-lattice parameter of the Cr<sub>2</sub>Te<sub>3</sub> layer of sample #2 is 12.304 Å. The thickness dependence of the c-lattice parameter of the layer peak was further studied among

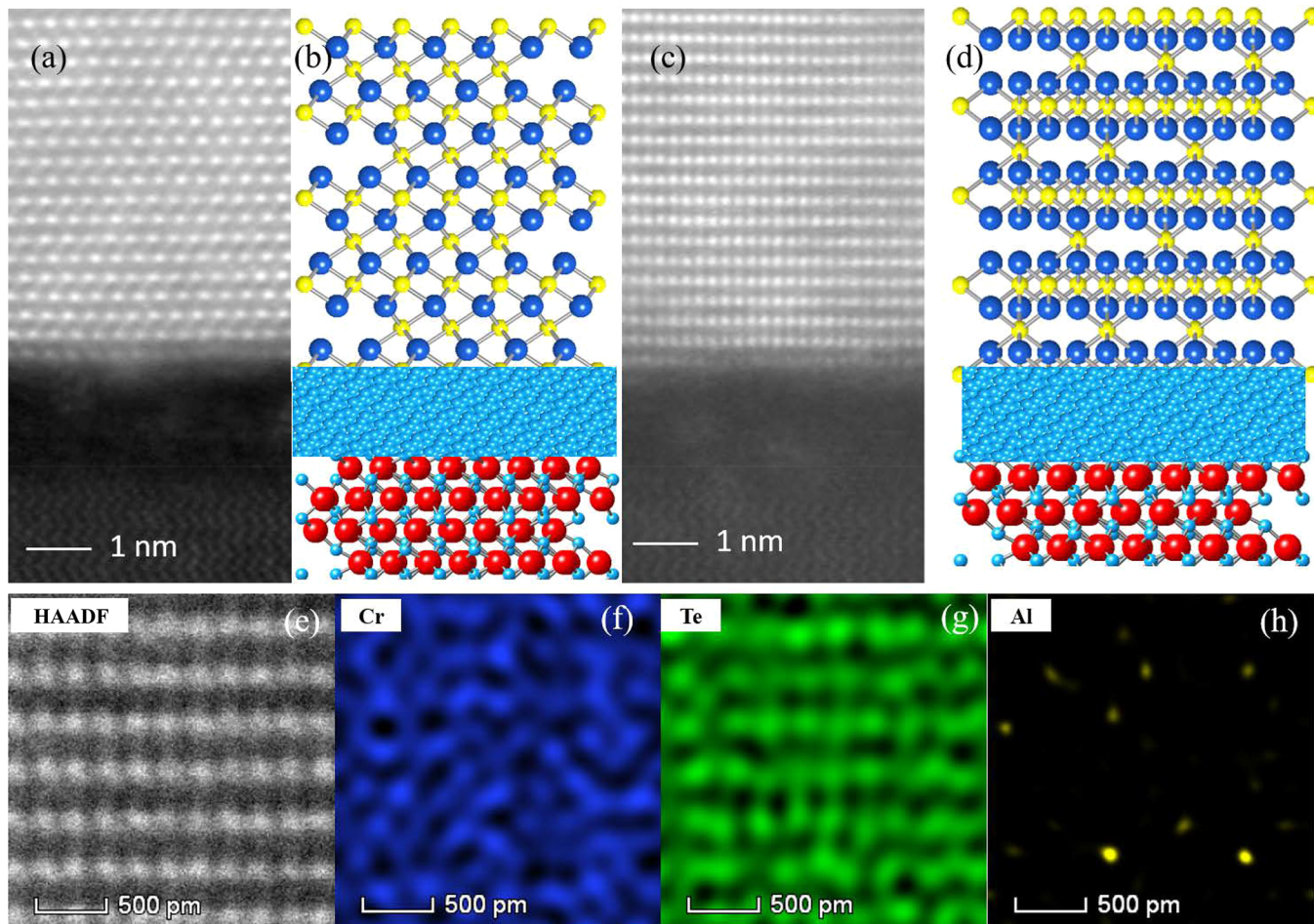


**Figure 4.** High-angle annular dark field (HAADF) scanning transmission electron microscopy (STEM) images and EDX mapping results of a  $\text{Cr}_2\text{Te}_3$  sample. (a,c) The cross-sectional STEM pictures of the interface. (b,d) The structures simulation corresponding to (a,c) respectively. (e) An area selected in (c) used for EDX mapping. (f,g,h) EDX mapping of Cr, Te, and Al obtained from the area shown in (e).

the four  $\text{Cr}_2\text{Te}_3$  samples. Figure 2b shows the XRD (008) peaks of these samples (samples #1 ~ #4) with their *c*-lattice parameters determined to be 12.255, 12.304, 12.309, and 12.327 Å, indicating that the *c*-lattice parameter increases with sample thickness. It is worthwhile to note that all these values are larger than the reported *c*-lattice parameter of bulk hexagonal  $\text{Cr}_2\text{Te}_3$ , which is 12.07 Å.<sup>19</sup> We believe that this difference may be caused by unexpected Al incorporation in the layers through diffusion from the  $\text{Al}_2\text{O}_3$  substrate, which will be addressed later.

The magnetization versus temperature ( $M-T$ ) curve from 2 to 320 K under an applied field of  $H = 1000$  Oe perpendicular to the surface and resistance versus temperature ( $R-T$ ) curve from 2 to 300 K for sample #2 are shown in Figure 3a. Both the  $M-T$  and  $R-T$  curves show a typical behavior of ferromagnetism around their para-ferro transition upon cooling. the Curie temperature is obtained by performing the first derivation of these curves. As shown in Figure 3b, the peak and valley at 244 K in the derivative curves indicate the Curie temperature at which magnetization and resistance change abruptly. We have carried out similar studies for the other samples. Figure 3c displays the  $M-T$  curves for all four samples, in which sample #4 was under a magnetic field of 50 Oe to show a clearer low-temperature behavior, which may due to its strong magnetic anisotropy. These  $M-T$  curves show that a tuning of Curie temperature from 165 to 295 K can be

achieved by varying their thicknesses that somehow might be related to the *c*-lattice parameter as illustrated in Figure 2b. In the following paragraphs, we will present the results of further structural, magnetic, and magneto-transport measurements to address the underlying mechanism of the observed tunability of the Curie temperature of our  $\text{Cr}_2\text{Te}_3$  samples.

Figure 4 displays the typical cross-sectional HAADF STEM images near the interface between  $\text{Cr}_2\text{Te}_3$  and  $\text{Al}_2\text{O}_3$  viewing along the  $[11\bar{2}0]$  direction of  $\text{Al}_2\text{O}_3$ , cutted from a  $\text{Cr}_2\text{Te}_3$  sample with a same thickness of sample #2, while a ZnSe layer was capped for protection purpose. Two types of domains with different orientations of  $\text{Cr}_2\text{Te}_3$ , one along the  $[110]$  direction (Figure 4a) and the other along the  $[\bar{1}\bar{2}0]$  direction (Figure 4c) are found. As estimated from all the available TEM images, we found that more domains that atoms arranged like Figure 4c were found than those arranged like Figure 4a. Structural simulations for both STEM images are given accordingly in Figure 4b,d. It should be noted that an amorphous layer with thickness ~2 nm has been observed at the interface between the  $\text{Cr}_2\text{Te}_3$  layer and the  $\text{Al}_2\text{O}_3$  substrate for both domain types. Chemical composition characterization of the  $\text{Cr}_2\text{Te}_3$  layer in the area far away from the interface is performed by EDX installed in the STEM. Figure 4e displays the STEM image from a domain like the one shown in Figure 4c, which is used for this characterization. The resulted mapping for Cr, Te, and Al are shown in panels f, g, and h, respectively, of Figure 4.

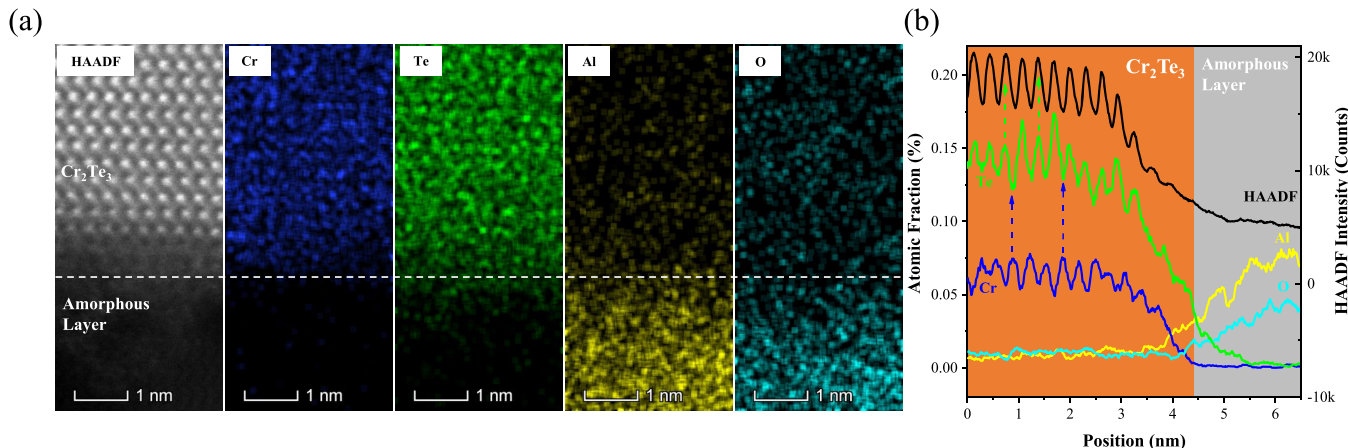


**Figure 5.** (HAADF) STEM images and EDX mapping analysis of the interface between  $\text{Cr}_2\text{Te}_3$  and the amorphous layer. (a)  $\text{Cr}_2\text{Te}_3/\text{Al}_2\text{O}_3$  interface used for EDX mapping and its corresponding EDX mapping of Cr, Te, Al, and O element, respectively. (b) EDX mapping profile of (a), showing the relation of HAADF intensity and atomic fraction of Cr, Te, Al, and O elements versus the vertical position of interface. The horizontal-axis is the distance to the starting point of the image bottom, the approximate positions of the amorphous layer could be distinguished by the sudden drop of Te elements. Noticeably, the peaks of the Te match with the peaks of HAADF intensity curve as the green arrows indicated. Moreover, the peak of Cr located exactly at the valley of Te as the blue arrows indicated, demonstrating the Cr–Te–Cr layered structure of  $\text{Cr}_2\text{Te}_3$ , the excess Al atomic fraction in the amorphous layer suggesting an O-deficient phase from  $\text{Al}_2\text{O}_3$ .

The distribution of Te element shown in Figure 4g is in good consistency with the STEM graph shown in Figure 4e. The Cr atom which is invisible in the TEM graph because of its small atomic radius, can be observed in the EDX mapping. The EDX mapping result of Cr atoms (Figure 4f) shows that Cr atoms represented by relative bright blue dots are interspersed between Te atoms, consistent with the structure as shown in Figure 4d. Besides Cr and Te elements, a small amount of Al is identified in Figure 4h.

To determine the composition of the amorphous layer shown in Figure 4, we performed atomic-scale EDX mapping at the interface region. The STEM graph taken in HAADF mode is shown in Figure 5a, showing the atomic structure and distribution of elements of the interface. In Figure 5a, we scan lines across the interface (amorphous layer) sandwiched between the  $\text{Cr}_2\text{Te}_3$  layer and the  $\text{Al}_2\text{O}_3$  substrate. The corresponding distributions of the Cr, Te, Al, and O atomic fractions along the line are shown in Figure 5b, with the HAADF intensity also added for assisting the chemical analysis, in which the oscillations of Te and Cr atomic fraction curve dropped abruptly at the interface of the amorphous layer, followed with a rising chemical composition of Al and O, manifesting a sharp interface between  $\text{Cr}_2\text{Te}_3$  and the amorphous layer. Surprisingly, we observe a significant Al abundance (with the ratio nearly  $\text{Al}:\text{O} \approx 2:1$ ) in the amorphous layer, indicating that the amorphous layer is likely an Al-dominated layer, and the thickness is about 2 nm. A similar observation for the growth of GaN on  $\text{Al}_2\text{O}_3$  has been reported by Wenliang Wang et al.<sup>20</sup> They named it as nitridation effect of  $\text{Al}_2\text{O}_3$ . To investigate the formation mechanism of the unknown Al dominated amorphous layer, we further performed a control experiment by growing the  $\text{Cr}_2\text{Te}_3$  at a lower temperature around 300 K. The structure analysis is shown in Supporting Information (Figure S1), in which the amorphous layer does not exist at the interface. Hence, in our  $\text{Cr}_2\text{Te}_3$  sample, we could speculate that the tellurium-rich environment and high substrate temperature during the sample growth may play important roles for causing

the top few layers of the  $\text{Al}_2\text{O}_3$  substrate to suffer from oxygen deficiency.

Noticeably, the “noise” of the O element in Figure 5a is quite large in the  $\text{Cr}_2\text{Te}_3$  layer. However, it could not prove that the O element diffused into the top layer, and there are two reasons may illustrate the existence of the O element at the top part: First, there is still a little “noise” that exists due to the  $\text{Al}_2\text{O}_3$  substrate background. Second, commonly, there exists much contamination of the O element from the air; thus, the O element should be ubiquitous on the surface of STEM sample. However, we still could estimate that the O element is not incorporated into the  $\text{Cr}_2\text{Te}_3$  lattice from the EDX results shown in Figure 5b, as we could clearly observe that the O element curve is nearly uniform and the O element randomly distributes at  $\text{Cr}_2\text{Te}_3$  layer as shown in Figure 5b. This may suggest the O element is coming from the contaminations, while the Al curve shows a decline, which is a typical shape for diffusion. In contrast, as to the Al signal at the top region, we still could observe the Al elemental signal in Figure 4h, which is relatively far away from the interface of  $\text{Cr}_2\text{Te}_3$  and  $\text{Al}_2\text{O}_3$ . Since the environment contains no Al element, hereby, we could be sure that the Al element is diffused into the  $\text{Cr}_2\text{Te}_3$  lattice from the interface. In this report, we believe the influence of the O element to  $\text{Cr}_2\text{Te}_3$  should be negligible because the sample is exposed to the air for measurements, and its properties do not vary within a considerable long time. Thus, we focus the main concern here on the Al incorporation caused by the diffusion effect.

Now let us revisit the observed Al contamination in our  $\text{Cr}_2\text{Te}_3$  layers and see how it may affect the electrical transport of these layers. To our best knowledge, the conduction type of all  $\text{Cr}_2\text{Te}_3$  bulk or thin film materials reported previously is p-type.<sup>5</sup>  $\text{Cr}_2\text{Te}_3$  samples grown on ZnSe in our group using the same MBE system also constantly show a p-type feature.<sup>21</sup> To investigate the effect of Al contamination, A six-terminal Hall bar device was fabricated on a small piece of sample #2 for performing magneto-transport measurements. The width and length of the device are 1000 and 500  $\mu\text{m}$ , respectively. Its Hall resistivity was derived from the voltage along the XY direction

with a current of  $50 \mu\text{A}$  flowing along the XX direction. The results of Hall effect measurements performed on sample #2 are shown in **Figure 6** with  $\rho_{yx}(H)$  curves having been offset

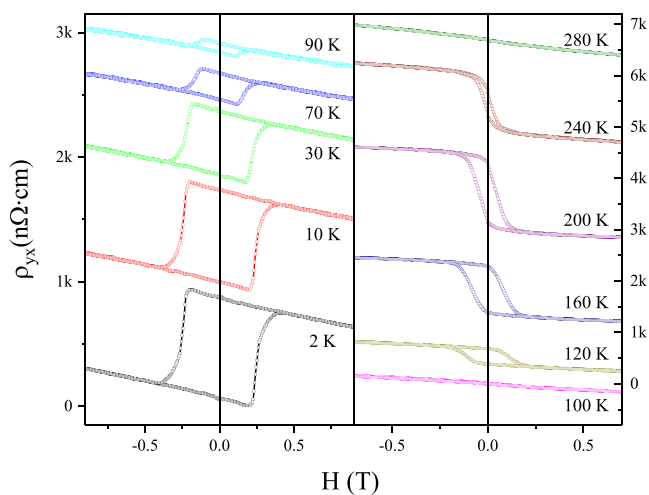


**Figure 6.** Results of Hall effect measurements performed on sample #2. Showing the temperature dependent  $\rho_{yx}$  vs magnetic field strength from 2 to 280 K of sample #2.

vertically for clarity. At 280 K, the measured Hall resistivity is linearly dependent on H field, which is a typical feature of ordinary Hall effect (OHE). However, below the Curie temperature (244 K), a clear hysteresis behavior is observed, which is an indicator of the anomalous Hall effect (AHE) that arises from the ferromagnetic ordering with PMA property. At low temperature, the hysteresis loop narrows and vanishes at 100 K. As temperature decreases further,  $\rho_{yx}$  reverses its sign compared with  $\rho_{yx}$  measured at temperature above 100 K. The observed temperature-dependent AHE is related to several transport mechanisms of the charge carriers,<sup>22</sup> including the extrinsic (skew scattering, side jump) and intrinsic (Berry phase) that could cause the AHE.<sup>23</sup> Those mechanisms will compete with each other, leading to the “sign-reversal” feature observed in **Figure 6** (the details of our analysis will be reported elsewhere). Here, we would like to focus on the observation that the overall Hall resistance show decreasing tendency with increasing magnetic field, as shown in **Figure 6b**, which indicates that sample #2 have n-type carriers. The carrier concentration is derived by linearly fitting the Hall resistance  $\rho_{yx}$  to magnetic field at large magnetic field values (ordinary hall effect dominating region), which is estimated to be about  $10^{21} \text{ cm}^{-3}$  for sample #2. We also performed Hall measurement of the control sample shown in **Supporting Information** (a  $\text{Cr}_2\text{Te}_3$  thin film grown on  $\text{Al}_2\text{O}_3$  substrate without Al rich amorphous layer), in which p-type hall conductance was shown unambiguously (**Figure S2**). All above results lead us to believe that the observed Al-rich interface layer and incorporation of Al atoms in  $\text{Cr}_2\text{Te}_3$  lattice may cause our  $\text{Cr}_2\text{Te}_3$  thin films grown on  $\text{Al}_2\text{O}_3$  substrate to be n-type, possibly by contributing free electrons from the Al atoms.

The magnetic hysteresis loop measured for sample #2 is shown in **Figure 7**. The measured magnetization curve (M–H curve) with the applied magnetic field perpendicular to the sample surface shows a square shaped loop with coercive force around 0.25 T and shifts into a round shape when the applied magnetic field is parallel to the sample surface, indicating that the sample has uniaxial anisotropy with easy axis perpendicular

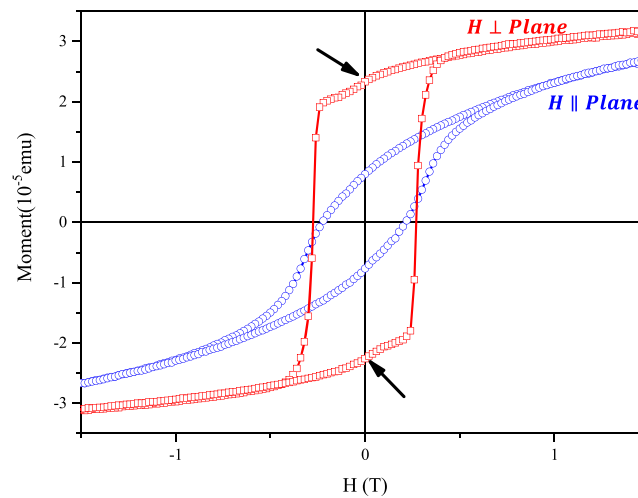


**Figure 7.** M–H curves of sample #2 with magnetic field perpendicular and parallel to the surface respectively measured at 2.1 K. The black arrows indicate the small step-like kinks.

to the plane, consistent with previous reports on the easy axis of  $\text{Cr}_2\text{Te}_3$  compound.<sup>7</sup> However, the hysteresis loop is not saturated with magnetic field up to 1.5 T, indicating the relatively large anisotropy of  $\text{Cr}_2\text{Te}_3$  may be due to the heavy element Te and low symmetry of the crystal lattice.<sup>24,25</sup> In **Figure 7**, a small step-like kink feature around the zero-field region is found in the hysteresis loop for the out-of-plane direction, which is usually observed in complicated magnetic systems with composite ordering, such as ferrimagnetic or ferromagnetic materials inclusion with different switching fields. Noticeably, Wang et al. have also observed such kink in  $\text{Cr}_2\text{Te}_3$  nanorods, which could be ascribed to spatial inhomogeneity of the nanorods.<sup>26</sup> Similarly, via TEM images of **Figure 4**, we have demonstrated that some rotation domains exist in our  $\text{Cr}_2\text{Te}_3$  thin film. Hereby, we believe that the grain boundary of  $\text{Cr}_2\text{Te}_3$  rotation domain may attribute to the kink in MH loop; however, the details of the formation mechanism of the kink are still unrevealed, which is worthy for the further study.

To study the magnetization properties of  $\text{Cr}_2\text{Te}_3$  thin films, zero field cooled (ZFC) and field cooled (FC) M–T curves are measured simultaneously. **Figure 8a** shows the ZFC and FC curves of sample #2 with a magnetic field perpendicular to the sample surface with the magnitude of 100, 500, 1000, and 2000 Oe, respectively. FC curves were measured while cooling down from 320 K. ZFC curves were measured while warming up with the same magnetic field used for measuring FC curves after they were cooled from 320 K without a magnetic field. The obtained FC magnetization curves correspond to a typical magnetization behavior of ferromagnetism. The ZFC curves display an increase of magnetization when warming up from 2 K for all curves, followed by a decrease of magnetization after a characteristic temperature, and eventually merge with the FC magnetization curves at a blocking temperature  $T_b$ . With increasing magnetic field, the blocking temperature decreases. This temperature-dependent magnetization behavior is similar to the typical behavior of spin-glass or spin-cluster. Noted that the spin-glass or spin-cluster should be distinguished by the decaying magnetic remanence moments after withdrawing external magnetic field.<sup>27</sup> To verify this feature, magnetic remanence ( $M_r$ ) of sample #2 was conducted at 2.1 K after applying a 2 T magnetic field perpendicular to the sample

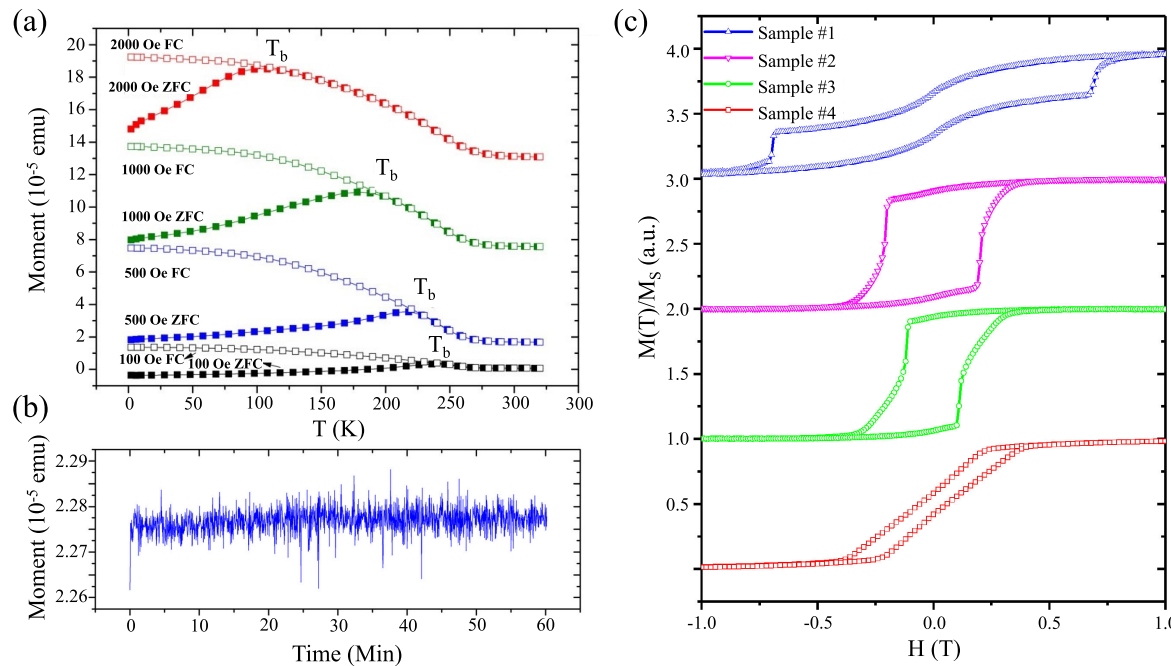


**Figure 8.** Results of various magnetic moment measurements performed on  $\text{Cr}_2\text{Te}_3$  samples. (a) ZFC and FC curves of sample #2 with magnetic field perpendicular to the surface. (b) Magnetic remanence ( $M_r$ ) of sample #2 at 2.1 K after applying a 2 T magnetic field perpendicular to the sample surface and withdrawing back to zero quickly. (c) Magnetic hysteresis loops measured for sample #1–#4 with magnetic field perpendicular to the surface at 2 K.

surface and withdrawing back to zero quickly (Figure 8b), in which the out of plane  $M_r$  stays at a constant value with measuring time at least up to 60 min, which is a signature of nondecay ferromagnetic ordering but not spin glass. Thus, we believed that the occurrence of discrepancy in ZFC and FC  $M-T$  curves of sample #2 are likely not a signature of pure spin-glass or spin cluster, hereby, we believe that the magnetization behavior in Figure 8a is due to antiferromagnetic/ferromagnetic coexistence in  $\text{Cr}_2\text{Te}_3$ . In fact, it is consistent with previous research on the chromium telluride system, which experimentally show that in the Cr fully occupied layer of chromium telluride, moments are ferromagnetically ordered,<sup>5</sup> while in the Cr vacancy layer, the moments are antiferromagnetically ordered.<sup>2,4,28,29</sup>

To investigate the details of the magnetic ordering in our samples, magnetic hysteresis loops of sample #1–#4 were shown in Figure 8c, in which the magnetic moments are normalized to  $-1$  to  $1$  and offset vertically for clarity. We could clearly observe the kink disappears and coercive field decreases with the thin film thickness increasing, in which the former feature could result from the reduction of rotation domain during the thin film growth process. Our thickness-dependent structural analysis (Figure 2) shows that, with increasing thin film thickness, the distance between the interatomic layers stacking along [001] direction of  $\text{Cr}_2\text{Te}_3$  gets larger, weakening the interaction between the Cr vacancy layer and the fully occupied layer. Considering the small AFM ordering exists in the Cr vacancy layer, with increasing distance between the atomic layers, the coupling between FM ordering and AFM ordering is expected to be weakened either. Thus, it is easier for moments ferromagnetically ordered to be aligned to the external magnetic field, which may serve as the mechanism for explaining the  $H_C$  and Curie temperature dependence on the thickness in Figure 8c and Figure 3c. It is worth noting that

previous high-pressure studies on  $\text{Cr}_2\text{Te}_3$  samples grown by other methods indicate that the Curie temperature decreases with the contraction of  $c$ -axis.<sup>30,31</sup> In our work, the observed enhancement of  $T_C$  in our samples can be attributed to the same mechanism with an opposite direction that the  $c$ -axis is extended.

Combining the transport and magnetic measurement results, we observe an unusual thickness dependent  $c$ -axis variation in our n-type  $\text{Cr}_2\text{Te}_3$  with higher Curie temperature, which is absent of reported in previous study on the p-type  $\text{Cr}_2\text{Te}_3$  thin films grown on the ZnSe or Si substrates, clearly in which no Al diffusion occurs in the  $\text{Cr}_2\text{Te}_3$  lattice (Figure S1). Since the major difference between the n-type and p-type  $\text{Cr}_2\text{Te}_3$  is the Al incorporation caused by interfacial diffusion, hereby we would like to attribute the lattice constant dependence on thickness to the diffusion of Al atoms, which may cause the inflation of  $c$ -axis in our sample. However, such speculation deserves a systematic study by directly doping Al into the  $\text{Cr}_2\text{Te}_3$  thin film in the future, which may also provide a controllable way for adjusting the curie temperature of  $\text{Cr}_2\text{Te}_3$ .

## CONCLUSIONS

In this work, MBE-grown hexagonal  $\text{Cr}_2\text{Te}_3$  thin films grown on  $\text{Al}_2\text{O}_3$  substrates were found to have high Curie temperature. In situ long streaky reflection high-energy electron diffraction patterns observed in the  $\text{Cr}_2\text{Te}_3$  thin films indicate that they were grown with atomically flat surface with high crystalline quality. It was found that a 2 nm amorphous layer of Al exists at the interface between  $\text{Cr}_2\text{Te}_3$  and  $\text{Al}_2\text{O}_3$ , and a small amount of Al contamination is incorporated into the  $\text{Cr}_2\text{Te}_3$  layer, which induces the n-type conduction type of our samples in contrast to the p-type signature observed for  $\text{Cr}_2\text{Te}_3$  samples as reported by others previously. A phenomenological model for the coupling

between FM ordering and AFM ordering that exists in our  $\text{Cr}_2\text{Te}_3$  thin films is proposed on the basis of the results of the magnetic characterizations performed on them. The phenomenon that Curie temperature increases as the c-lattice parameter increases can be explained using our proposed phenomenological model.

## ■ ASSOCIATED CONTENT

### Supporting Information

The Supporting Information is available free of charge on the ACS Publications website at DOI: [10.1021/acsanm.9b01179](https://doi.org/10.1021/acsanm.9b01179).

Stoichiometry analysis; HRTEM, R-T, Hall measurement of the  $\text{Cr}_2\text{Te}_3$  sample without amorphous layer ([PDF](#))

## ■ AUTHOR INFORMATION

### Corresponding Authors

\*E-mail: [phiksou@ust.hk](mailto:phiksou@ust.hk).

\*E-mail: [wangg@sustech.edu.cn](mailto:wangg@sustech.edu.cn).

### ORCID

Hongxi Li: [0000-0002-9492-6220](https://orcid.org/0000-0002-9492-6220)

Junshu Chen: [0000-0003-2295-772X](https://orcid.org/0000-0003-2295-772X)

Hongtao He: [0000-0001-6748-874X](https://orcid.org/0000-0001-6748-874X)

Gan Wang: [0000-0002-4364-2885](https://orcid.org/0000-0002-4364-2885)

### Present Address

<sup>†</sup>H.L.: Department of Physics and Astronomy, 525 Northwestern Avenue, West Lafayette, IN 47907, United States

### Author Contributions

#H.L., L.W. and J.C.: These authors contributed equally.

### Funding

This work was supported by the National Natural Science Foundation of China (No. 11774143), the National Key Research and Development Program of China (No. 2018YFA0307100, No.2016YFA0301703), the Natural Science Foundation of Guangdong Province (No.2015A030313840, No.2017A030313033), the State Key Laboratory of Low-Dimensional Quantum Physics (No.KF201602), Technology and Innovation Commission of Shenzhen Municipality (KQJSCX20170727090712763, ZDSYS20170303165926217, and JCYJ20170412152334605).

### Notes

The authors declare no competing financial interest.

## ■ REFERENCES

- (1) Atkinson, R. Optical and Magneto-Optical Properties of Thin Film Chromium Telluride. *Thin Solid Films* **1977**, *47* (2), 177–186.
- (2) Dijkstra, J.; van Bruggen, C.; Haas, C.; de Groot, R. Electronic Band-Structure Calculations of Some Magnetic Chromium Compounds. *J. Phys.: Condens. Matter* **1989**, *1* (46), 9163.
- (3) Hashimoto, T.; Yamaguchi, M. Magnetic Properties of  $\text{Cr}_7\text{Te}_8$ . *J. Phys. Soc. Jpn.* **1969**, *27* (5), 1121–1126.
- (4) Andresen, A. F.; Zeppezauer, E.; Boive, T.; Nordstrom, B.; Branden, C.-I. The Magnetic Structure of  $\text{Cr}_2\text{Te}_3$ ,  $\text{Cr}_3\text{Te}_4$ , and  $\text{Cr}_5\text{Te}_6$ . *Acta Chem. Scand.* **1970**, *24* (10), 3495–3509.
- (5) Dijkstra, J.; Weitering, H.; van Bruggen, C.; Haas, C.; De Groot, R. Band-Structure Calculations, and Magnetic and Transport Properties of Ferromagnetic Chromium Tellurides ( $\text{CrTe}$ ,  $\text{Cr}_3\text{Te}_4$ ,  $\text{Cr}_2\text{Te}_3$ ). *J. Phys.: Condens. Matter* **1989**, *1* (46), 9141–9161.
- (6) Kanazawa, K.; Yamawaki, K.; Sekita, N.; Nishio, Y.; Kuroda, S.; Mitome, M.; Bando, Y. Structural and Magnetic Properties of Hexagonal  $\text{Cr}_{1-\delta}\text{Te}$  Films Grown on CdTe (001) by Molecular Beam Epitaxy. *J. Cryst. Growth* **2015**, *415*, 31–35.
- (7) Roy, A.; Guchhait, S.; Dey, R.; Pramanik, T.; Hsieh, C.-C.; Rai, A.; Banerjee, S. K. Perpendicular Magnetic Anisotropy and Spin Glass-Like Behavior in Molecular Beam Epitaxy Grown Chromium Telluride Thin Films. *ACS Nano* **2015**, *9* (4), 3772–3779.
- (8) Pramanik, T.; Roy, A.; Dey, R.; Rai, A.; Guchhait, S.; Movva, H. C.; Hsieh, C.-C.; Banerjee, S. K. Angular Dependence of Magnetization Reversal in Epitaxial Chromium Telluride Thin Films with Perpendicular Magnetic Anisotropy. *J. Magn. Magn. Mater.* **2017**, *437*, 72–77.
- (9) Akiyama, R.; Oikawa, H.; Yamawaki, K.; Kuroda, S. Electric-Field Modulation of Ferromagnetism in Hexagonal Chromium Telluride Thin Film. *physica status solidi (c)* **2014**, *11* (7–8), 1320–1323.
- (10) Saito, H.; Yuasa, S.; Ando, K. Tunnel Magnetoresistance Effect in  $\text{Cr}_{1-\delta}\text{Te}/\text{AlAs}/\text{Ga}_{1-x}\text{Mn}_x\text{As}$  Magnetic Tunnel Junctions. *J. Appl. Phys.* **2005**, *97* (10), 10D305.
- (11) Zhao, D.; Zhang, L.; Malik, I. A.; Liao, M.; Cui, W.; Cai, X.; Zheng, C.; Li, L.; Hu, X.; Zhang, D.; et al. Observation of Unconventional Anomalous Hall Effect in Epitaxial CrTe Thin Films. *Nano Res.* **2018**, *11* (6), 3116–3121.
- (12) Chen, J.; Wang, L.; Zhang, M.; Zhou, L.; Zhang, R.; Jin, L.; Wang, X.; Qin, H.; Qiu, Y.; Mei, J.; Ye, F.; Xi, B.; He, H.; Li, B.; Wang, G. Evidence for Magnetic Skyrmions at the Interface of Ferromagnet/Topological-Insulator Heterostructures. *Nano Lett.* **2019**, *19* (9), 6144–6151.
- (13) Zhou, L.; Chen, J.; Chen, X.; Xi, B.; Qiu, Y.; Zhang, J.; Wang, L.; Zhang, R.; Ye, B.; Chen, P. 2019, Topological Hall Effect in Bulk Ferromagnet  $\text{Cr}_2\text{Te}_3$  Embedded with Black-Phosphorus-Like Bismuth Nanosheets. *arXiv preprint arXiv:1903.06486*. arXiv.org e-Print archive. <https://arxiv.org/abs/1903.06486>.
- (14) Bi, J.; Sreenivasan, M.; Teo, K.; Liew, T. Observation of Strong Magnetic Anisotropy in Zinc-Blende CrTe Thin Films. *J. Phys. D: Appl. Phys.* **2008**, *41* (4), 045002.
- (15) Hui, L.; Lim, S.; Bi, J.; Teo, K. Investigation on the Antiferromagnetic Component in the Intrinsic Exchange Bias in Structurally Single Phase  $\text{Cr}_2\text{Te}_3$  Thin Film. *J. Appl. Phys.* **2012**, *111* (7), 07D719.
- (16) Sreenivasan, M.; Bi, J.; Teo, K.; Liew, T. Systematic Investigation of Structural and Magnetic Properties in Molecular Beam Epitaxial Growth of Metastable Zinc-Blende CrTe toward Half-Metallicity. *J. Appl. Phys.* **2008**, *103* (4), 043908.
- (17) Sreenivasan, M.; Teo, K.; Jalil, M.; Liew, T.; Chong, T.; Du, A. Zinc-Blende Structure of CrTe Epilayers Grown on GaAs. *IEEE Trans. Magn.* **2006**, *42* (10), 2691–2693.
- (18)  $\alpha\text{-Al}_2\text{O}_3$ , corundum ( $\text{Al}_2\text{O}_3$ ) Crystal Structure: Datasheet from “PAULING FILE Multinaries ed. – 2012” in SpringerMaterials ([https://materials.springer.com/isp/crystallographic/docs/sd\\_1221826](https://materials.springer.com/isp/crystallographic/docs/sd_1221826)), Springer-Verlag Berlin Heidelberg & Material Phases Data System (MPDS), Switzerland & National Institute for Materials Science (NIMS), Japan, [Accessed on 27 January 2019].
- (19)  $\text{Cr}_2\text{Te}_3$  Crystal Structure: Datasheet from “PAULING FILE Multinaries ed. – 2012” in SpringerMaterials ([https://materials.springer.com/isp/crystallographic/docs/sd\\_0260160](https://materials.springer.com/isp/crystallographic/docs/sd_0260160)), Springer-Verlag Berlin Heidelberg & Material Phases Data System (MPDS), Switzerland & National Institute for Materials Science (NIMS), Japan, [Accessed on 27 January 2019].
- (20) Wang, W.; Liu, Z.; Yang, W.; Lin, Y.; Zhou, S.; Qian, H.; Wang, H.; Lin, Z.; Li, G. Nitridation Effect of the  $\alpha\text{-Al}_2\text{O}_3$  Substrates on the Quality of the GaN Films Grown by Pulsed Laser Deposition. *RSC Adv.* **2014**, *4* (75), 39651–39656.
- (21) Zhou, L.; Chen, J.; Du, Z.; He, X.; Ye, B.; Guo, G.; Lu, H.; Wang, G.; He, H. Magnetotransport Properties of  $\text{Cr}_{1-\delta}\text{Te}$  Thin Films with Strong Perpendicular Magnetic Anisotropy. *AIP Adv.* **2017**, *7* (12), 125116.
- (22) Kovalev, A. A.; Tserkovnyak, Y.; Výborný, K.; Sinova, J. Transport Theory for Disordered Multiple-Band Systems: Anomalous Hall Effect and Anisotropic Magnetoresistance. *Phys. Rev. B: Condens. Matter Mater. Phys.* **2009**, *79* (19), 195129.

- (23) Nagaosa, N.; Sinova, J.; Onoda, S.; MacDonald, A. H.; Ong, N. P. Anomalous Hall Effect. *Rev. Mod. Phys.* **2010**, *82* (2), 1539.
- (24) Zhang, H.; Long, G.; Li, D.; Sabirianov, R.; Zeng, H. Fe<sub>3</sub>Se<sub>4</sub> Nanostructures with Giant Coercivity Synthesized by Solution Chemistry. *Chem. Mater.* **2011**, *23* (16), 3769–3774.
- (25) Long, G.; Zhang, H.; Li, D.; Sabirianov, R.; Zhang, Z.; Zeng, H. Magnetic Anisotropy and Coercivity of Fe<sub>3</sub>Se<sub>4</sub> Nanostructures. *Appl. Phys. Lett.* **2011**, *99* (20), 202103.
- (26) Wang, F.; Du, J.; Sun, F.; Sabirianov, R. F.; Al-Aqtash, N.; Sengupta, D.; Zeng, H.; Xu, X. Ferromagnetic Cr<sub>2</sub>Te<sub>3</sub> Nanorods with Ultrahigh Coercivity. *Nanoscale* **2018**, *10* (23), 11028–11033.
- (27) Nordblad, P.; Lundgren, L.; Sandlund, L. A Link between the Relaxation of the Zero Field Cooled and the Thermoremanent Magnetizations in Spin Glasses. *J. Magn. Magn. Mater.* **1986**, *54*, 185–186.
- (28) Hamasaki, T.; Hashimoto, T.; Yamaguchi, Y.; Watanabe, H. Neutron Diffraction Study of Cr<sub>2</sub>Te<sub>3</sub> Single Crystal. *Solid State Commun.* **1975**, *16* (7), 895–897.
- (29) Hashimoto, T.; Hoya, K.; Yamaguchi, M.; Ichitsubo, I. Magnetic Properties of Single Crystals Cr<sub>2-δ</sub>Te<sub>3</sub>. *J. Phys. Soc. Jpn.* **1971**, *31* (3), 679–682.
- (30) Kanomata, T.; Sugawara, Y.; Kamishima, K.; Mitamura, H.; Goto, T.; Ohta, S.; Kaneko, T. Pressure Effect on Spontaneous Magnetization of Cr<sub>2</sub>Te<sub>3</sub> and Cr<sub>5</sub>Te<sub>8</sub>. *J. Magn. Magn. Mater.* **1998**, *177*, 589–590.
- (31) Yuzuri, M.; Kanomata, T.; Kaneko, T. The Pressure Effect on the Curie Temperature and Exchange Striction of Cr<sub>2</sub>S<sub>3</sub> and Cr<sub>2</sub>Te<sub>3</sub>. *J. Magn. Magn. Mater.* **1987**, *70* (1–3), 223–224.